SIMPLIFIED CRITERIA FOR MINIMUM LOAD AND DRIFT CONTROL OF LARGE BOOSTER VEHICLE

HAYES INTERNATIONAL CORPORATION

BIRMINGHAM, ALABAMA

SIMPLIFIED CRITERIA FOR MINIMUM LOAD AND DRIFT CONTROL OF LARGE BOOSTER VEHICLE

ENGINEERING REPORT

NO. 1214

22 DECEMBER 1965

PREPARED BY:

D. L. St. John

APPROVED BY:

Harry Passmore, III
Project Engineer

C. L. Anker
Project Manager

P. R. Coulson
Program Manager

REVISIONS

DATE	PAGES AFFECTED	REMARKS	BY	APP.

ABSTRACT

24576

A re-evaluation of control system criteria for minimizing lateral drift and structural loading of large booster vehicles during launch is made. A simplified mathematical rigid body booster model, neglecting engine gimbal and accelerometer dynamics and employing lateral acceleration feedback, is used in the analysis in order that fundamental concepts can be simply illustrated. Basic understanding of the minimum drift and minimum load control criteria is obtained using a servo analysis approach in conjunction with statistical design techniques.

Simplified lateral drift and bending moment closed-loop transfer functions due to lateral wind disturbances are derived from application of root locus and frequency response analysis to the rigid booster model. Correlation of the simplified and exact transfer function representation of the vehicle response is accomplished with an approximate statistical model of the lateral wind input. Statistical techniques are used as an aid in determining basic criteria for minimum load and minimum drift control.

Criteria for minimum drift control are easily defined, while the criteria for minimum load control are not so apparent.

Mr. R. S. Ryan, Chief, Dynamics Analysis Branch of the Flight Mechanics and Dynamics Division of the Aero-Astrodynamics Laboratory was the technical supervisor and the work reported herein was accomplished under contract NAS8-20201 with the George C. Marshall Space Flight Center, National Aeronautics and Space Administration.

TABLE OF CONTENTS

LIST OF FIGURES

LIST OF SYMBOLS

a, b	Real zeros
a_o	Attitude loop gain of attitude control system
a_1	Rate loop gain of attitude control system
A	Lateral acceleration
BM	Rigid body bending moment
d_i	Coefficient of i-th order denominator term
F_o, F_1	Rigid vehicle aerodynamic coefficients
$F-X$	Thrust
F_s	Swivel engine thrust
g	Longitudinal acceleration of the vehicle
g_2	Gain of accelerator control loop
$G_{BM-BM}(\omega)$	Bending moment output power spectra
$G_{YY}(\omega)$	System output spectra
$G_{\dot{Y}\dot{Y}}(\omega)$	Lateral drift velocity output power spectra
I	Effective moment of inertia of the vehicle about the c. g.
L	Turbulence integral scale factor
m	Vehicle mass
M'_α	Bending moment coefficient for angle of attack
M'_β	Bending moment coefficient for engine deflection
n_i	Coefficient of i-th order numerator term
Q	Dynamic pressure
t	Time

LIST OF SYMBOLS

Continued

V	Vehicle velocity
V_w	Lateral wind velocity
X_E	Coordinate of engine gimbal point (measured positive from center of gravity towards the tail of the vehicle)
X_A	Accelerometer location
Y	Lateral translation of the rigid vehicle
$Y(\omega)$	System frequency response function
$\dot{Y}$	Lateral drift velocity of rigid vehicle
α	Rigid body angle of attack
β	Swivel angle (angle of the engine gimbal relative to the vehicle centerline at the gimbal point)
ϕ	Pitch angle of rigid vehicle relative to inertial space
σ_{BM}	Standard deviation (root-mean-square) of BM
$\sigma_{\dot{Y}}$	Standard deviation (root-mean-square) of Y
σ^2_w	Variance of the lateral wind input

Subscript

i	Indicated order

INTRODUCTION

The emphasis of current design philosophy regarding trajectory precision and structural loading of large booster vehicles places stringent demands upon the vehicle control system when atmospheric turbulence and gust disturbances are considered. Maximum lateral wind velocities of 75 meters per second in the region of maximum dynamic pressure during the boost phase are not unrealistic. Accordingly, the problem of specifying the control system necessary to achieve minimum lateral drift in combination with minimum structural loading has attracted much effort during the past decade.

While a number of complicated studies of the large booster control problem in the past have succeeded in specifying several control laws which approximately minimize lateral drift and structural loading simultaneously, none have yielded a simplified explanation of the basic principles involved in minimum drift and minimum load control. Such a fundamental understanding of the drift and load control tasks is of particular interest since the relation between minimum drift and minimum loading is complicated, and some compromise between drift minimization and load alleviation is usually necessary. The objective of this study is the development of simple criteria, for minimum drift and minimum load control of large booster vehicles, which lend a simple understanding to the booster control problem.

A large booster mathematical model, similar in size to the Saturn V launch vehicle as defined for the Apollo lunar landing mission, was selected for analysis. In consideration of achieving the best understanding of the fundamental problem, simplified, single axis, rigid body motions only, for a fixed time of flight in the maximum "q" region of the boost stage, were considered. Three control loops form the basic control configuration: (1) Pitch position, (2) pitch rate, and (3) lateral acceleration feedback. The approach used in this study to develop criteria for minimum drift and load essentially involves determination of the effect each loop closure has upon the pole-zero movement of the lateral drift and rigid body bending moment closed loop transfer functions.

Two techniques are utilized to attack the minimum drift and load control problem: (1) Servo analysis, including root locus, and frequency response, and (2) simple statistical system design techniques. Approximate factors are developed for the lateral drift per side wind input and rigid body bending moment per side wind input closed loop transfer functions, and these approximate factors are used to state criteria for minimizing drift and structural loading. Correlation of the criteria developed from the simplified transfer functions with exact results is accomplished with the aid of statistical methods for computing the mean squared lateral drift and mean squared bending moment.

RIGID BOOSTER CONTROL

Vehicle Mathematical Model

The vehicle mathematical model chosen for this study must account for two important aspects of the problem: (1) Representation of simplified vehicle dynamics and control, and (2) the lateral wind disturbance representation. The wind input is considered later in the section on statistical analysis. The vehicle equations of motion, which in this study include only rigid body dynamics, are derived using Lagrange's equations and a coordinate system having its origin at the center of gravity of the vehicle. The rigid body bending moment equation was derived by the mode acceleration method. The equations of motion describing lateral translation, pitch rotation, bending moment, and control of the vehicle are presented below.

Lateral Translation

$$m\ddot{Y} - mg\phi - F_s\beta - QF_o\alpha = 0 \tag{1}$$

Pitch Rotation

$$I\ddot{\phi} + F_s X_E \beta + QF_1 \alpha = 0 \tag{2}$$

Control Equation

$$\beta - a_o\phi - a_1\dot{\phi} - g_2 A = 0 \tag{3}$$

Lateral Acceleration

$$A - \ddot{Y} + g\phi = 0 \tag{4}$$

Angle of Attack

$$\alpha - \phi + \frac{\dot{Y}}{V} = \frac{V_w}{V} \tag{5}$$

Rigid Body Bending Moment

$$BM(x,t) = M'_{\alpha}(x,t)\,\alpha + M'_{\beta}(x,t)\beta \tag{6}$$

The control law used in this analysis provides the following feedbacks: (1) Pitch position for heading control, (2) pitch rate for heading loop damping, and (3) lateral acceleration for lateral drift and bending moment control. These control loops are shown in Figure 1. Other feedback quantities were not considered at this time.

A rigid body mathematical model of the Saturn V, as defined for the lunar landing mission, was selected for this study. Numerical values of the model parameters for a time, t = 80 seconds, in the region of maximum dynamic pressure are listed in Table I.

TABLE 1

RIGID BODY BOOSTER DATA (t = 80 seconds)

a_o = 0.48
(Nominal Configuration)

a_1 = 1.1

F-X = 35.145×10^6 nt.

F_s = 29.456×10^6 nt.

g = 21.103 m/sec^2

V = 525.743 m/sec

Q = 5.607×10^6

m = 1.665×10^6 kg.

I = 7.329×10^8 kg-m^2

X_E = 30.244 m.

F_o = 1.10

F_1 = -12.32

X_A = 0

M'_α = 1.15×10^8 nt-m at X = 25 m.

M'_β = 3.04×10^8 nt-m at X = 25 m.

Servo Analysis of the Rigid Booster Model

Root locus and frequency response techniques are used to investigate minimum drift and minimum load control and it will be shown that: (1) Minimum drift control, i.e., the minimization of lateral drift velocity due to lateral wind disturbances by feedback control, is defined approximately by the movement of a single real root of the vehicle characteristic equation, and (2) load control of the rigid body bending moment due to lateral wind inputs, can be defined approximately by one real pole-zero pair.

Determination of simplified criteria for minimum drift and minimum load control for various control configurations in terms of system closed loop poles and zeros is a primary objective of this analysis. Since the $\frac{\dot{Y}}{V_w}(s)$ and $\frac{BM}{V_w}(s)$ closed-loop transfer functions are characterized by the same characteristic equation, i.e., their denominators are identical, the vehicle lateral drift and bending moment are closely interrelated.

The characteristic equation of our rigid booster model is:

$$\Delta = d_3 S^3 + d_2 S^2 + d_1 S + d_o = 0, \qquad (7)$$

where:

$$d_3 = (m - g_2 F_s) I$$

$$d_2 = \left(m X_E F_s a_1 + \frac{Q F_o I}{V}\right)$$

$$d_1 = (X_E F_s Q F_o - F_s Q F_1)\left(\frac{a_1}{V} + g_2\right) + m(X_E F_s a_o + Q F_1)$$

$$d_o = \frac{1}{V}(X_E F_s Q F_o - F_s Q F_1)(a_o - g_2 g) - mgQF_1$$

For a nominal configuration ($a_o = 0.48$, $a_1 = 1.1$) of the booster control system, the characteristic equation becomes

$$\Delta = (1.22060\,S^3 + 1.64062\,S^2 + 0.61564\,S + 0.01149)\cdot 10^{15}$$
$$-g_2\,(21.5879\,S^3 - 7.52654\,S + 0.30211)\cdot 10^{15} = 0 \qquad (8)$$

In root locus form, equation (8) may be written

$$1 = 17.6864\,g_2\,\frac{(s-0.0401)(s-0.5692)(s+0.6094)}{(s+0.0196)(s+0.6622 \pm j0.1945)} \qquad (9)$$

Solution of equation (9) for some value of g_2 yields the closed-loop poles of both $\frac{\dot{Y}}{V_w}(s)$ and $\frac{BM}{V_w}(s)$.

Effect of positive acceleration feedback, g_2, on the closed-loop poles of the nominal configuration of equation (9) is illustrated in the complex s-plane root locus plot of Figure 2. For $g_2 = 0$, the real pole near the origin ($s = -0.0196$) is referred to as the lateral drift pole, and the two oscillatory poles ($s = -0.6622 \pm j0.1945$) are identified as the rigid body poles. Increasing positive acceleration feedback has a two-fold effect on the closed-loop poles: (1) the rigid body poles

become real as g_2 becomes larger than 0.0113, and (2) the lateral drift pole moves from a small negative real quantity to zero as g_2 approaches 0.038, and moves into the right half s-plane as g_2 is increased beyond 0.038. Driving the minimum drift pole to zero will be shown to give a minimum vehicle response to lateral wind disturbance.

From the rigid body mathematical model (equation 1-6) the $\frac{\dot{Y}}{V_w}(s)$ transfer function is derived to be:

$$\frac{\dot{Y}}{V_w}(s) = K \frac{n_2 S^2 + n_1 S + n_o}{\Delta} \tag{10}$$

where:

$$K = \frac{1}{V}$$

$$n_2 = QF_o I$$

$$n_1 = (X_E F_s QF_o - F_s QF_1)a_1$$

$$n_o = (X_E FsQF_o - F_s QF_1)(a_o - g_{2\,1}\, g) - mgQF_1$$

For low accelerometer gains $(g_2 < +0.0113)$ $\frac{\dot{Y}}{V_w}(s)$ is of the form

$$\frac{\dot{Y}}{V_w}(s) = K_o \frac{(s+a)^2 + \omega_a^2}{(s+\alpha)\left[(s+\beta)^2 + \omega_\beta^2\right]}, \tag{11}$$

and for higher accelerometer gains $(g_2 > +0.0113)$

$$\frac{\dot{Y}}{V_w}(s) = K_o \frac{(s+a)(s+b)}{(s+\alpha)(s+\beta)(s+\gamma)} \tag{12}$$

Using the numerical values of the rigid booster model (Table 1), the frequency response plot of $\frac{\dot{Y}}{V_w}(j\omega)$ for the nominal configuration (a_o=0.48, a_1=1.1) is shown in Figure 3 for variations in accelerometer gain. It is seen that as the acceleration feedback increases to g_2 = + 0.038, the magnitude of $\left|\frac{\dot{Y}}{V_w}(j\omega)\right|$ is attenuated below the control frequency (approximately 1 radian). This effect on the low frequency $\left|\frac{\dot{Y}}{V_w}(j\omega)\right|$ magnitude is due to the movement of the lateral drift pole from some small, real negative value to zero as the gain g_2 increases. The $\left|\frac{\dot{Y}}{V_w}(j\omega)\right|$ magnitude approaches a minimum when the accelerometer gain is increased to g_2 = + 0.038. Since the log magnitude of $\left|\frac{\dot{Y}}{V_w}(j\omega)\right|$ at the control frequency is approximately -40 decibels and decreasing at -20 decibels per decade for frequencies above the control frequency, effect of the lateral drift pole is the dominant factor in determining the lateral drift characteristic of the vehicle.

The rigid body bending moment transfer function is:

$$\frac{BM}{V_w}(s) = K \frac{n_3 S^3 + n_2 S^2 + n_1 S}{\Delta} \tag{13}$$

where:

$$K = \frac{1}{V}$$

$$n_3 = \left[mM'_\alpha - g_{2\,1}(F_s M'_\alpha - QF_o M'_\beta)\right] I$$

$$n_2 = m(X_E F_s M'_\alpha - QF_1 M'_\beta)a_1$$

$$n_1 = m(X_E F_s M'_\alpha - QF_1 M'_\beta)\, a_o$$

$\frac{BM}{V_w}(s)$ is of the form

$$\frac{BM}{V_w}(s) = K_o \frac{s\left[(s+c)^2 + \omega_c^2\right]}{(s+\alpha)\left[(s+\beta)^2+\omega_\beta^2\right]} \tag{14}$$

for low accelerometer gain ($g_2 < 0.0113$), and of the form

$$\frac{BM}{V_w}(s) = K_o \frac{s(s+c)(s+d)}{(s+\alpha)(s+\beta)(s+\gamma)} \tag{15}$$

for higher gain g_2 .

For the mathematical model (Table 1), the effect of positive lateral acceleration feedback on $\frac{BM}{V_w}(j\omega)$ (Nominal configuration; $a_o = 0.48, a_1 = 1.1$) is shown in the bode plot of Figure 4. The $\frac{BM}{V_w}(j\omega)$ transfer function as seen from Figure 4 decreases in magnitude below $\omega \doteq 1$ rad/sec. for increasing g_2 , while it increases in magnitude for increasing g_2 above $\omega \doteq 1$ rad/sec. Two trade-offs are evident: (1) Relative importance of low and high frequency range* effects on the transfer function magnitude, and (2) relative importance of lateral drift and/or structural loading.

---

* "Low" indicates those frequencies less than $\omega \doteq 1$rad/sec, and "high" denotes those frequencies greater than $\omega \doteq 1$ rad/sec; further reference in this report to this terminology should be interpreted accordingly.

The frequency range which is more important for alleviating the structural load is closely related to the frequency content (spectra) of the lateral wind input as will be shown later in this report.

SIMPLIFIED TRANSFER FUNCTIONS

Drift Control

In view of the dominant effect which certain roots of the rigid booster model characteristic equation have upon minimum drift and minimum load control, it is conceivable that the closed-loop $\frac{\dot{Y}}{V_w}(s)$ and $\frac{BM}{V_w}(s)$ transfer functions can be simplified significantly with little error. These simplified transfer functions will be an aid for clarifying the criteria for minimum drift and minimum load control. An approximate factorization of the $\frac{\dot{Y}}{V_w}(s)$ transfer function is

$$\frac{\dot{Y}}{V_w}(s) \doteq \left(\frac{1}{V}\cdot\frac{n_2}{d_3}\right)\frac{(s+a^*)^2 + w_a^2}{(s+\frac{D_o}{D_1})\left[(s+\beta^*)^2+\omega_\beta^2\right]} \tag{16}$$

when the rigid body poles are underdamped ($g_2 < 0.0113$), and

$$\frac{\dot{Y}}{V_w}(s) \doteq K\frac{(s+a)(s+b)}{(s+\alpha)(s+\beta)(s+\gamma)} \tag{17}$$

when the rigid body poles are overdamped ($g_2 > 0.0113$)

where:

$$K = \frac{1}{V}\cdot\frac{n_2}{d_3}$$

$$N_1 = \frac{n_1}{n_2}$$

$$N_o = \frac{n_o}{n_2}$$

$$D_2 = \frac{d_2}{d_3}$$

$$D_1 = \frac{d_1}{d_3}$$

$$D_o = \frac{d_o}{d_3}$$

$$a^* = \frac{N_1}{2}, \quad \omega_a^2 = N_o - \frac{N_1^2}{4}$$

$$a = \frac{N_1}{2} - \frac{1}{2}\sqrt{N_1^2 - 4N_o}$$

$$b = \frac{N_1}{2} + \frac{1}{2}\sqrt{N_1^2 - 4N_o}$$

$$\alpha = \frac{D_o}{D_1}$$

$$\beta^* = \frac{D_2}{2}, \quad \omega_\beta^2 = D_1 - \frac{D_2^2}{4}$$

$$\gamma = \frac{D_2}{2} + \frac{1}{2}\sqrt{D_2^2 - 4D_1}, \quad \beta = \frac{D_2}{2} - \frac{1}{2}\sqrt{D_2^2 - 4D_1}$$

Since, for our mathematical model, the lateral drift pole, α, dominates the lateral drift response, and since the pole-zero pair of $\frac{\dot{Y}}{V_w}(j\omega)$ in the high frequency range, i.e., the b-γ pair, has little effect upon lateral drift characteristic, the approximate $\frac{\dot{Y}}{V_w}(s)$ transfer function of equation (17) can be simplified to

$$\frac{\dot{Y}}{V_w}(j\omega) \doteq K \frac{(s+a)}{(s+\alpha)(s+\beta)} \tag{18}$$

where K, a, α, and β are given in equation (17).

Bode plots of the simplified $\frac{\dot{Y}}{V_w}(j\omega)$ transfer functions are shown in Figure 5.

Load Control

Using the same approach as used for approximating $\frac{\dot{Y}}{V_w}(s)$, the approximate closed-loop $\frac{BM}{V_w}(s)$ transfer function is

$$\frac{BM}{V_w}(s) \doteq \frac{1}{V}\cdot\frac{n_3}{d_3}\ \frac{s\left[(s+c^*)^2+\omega_c^2\right]}{(s+\frac{D_o}{D_1})\left[(s+\beta^*)^2+\omega_\beta^2\right]} \tag{19}$$

for underdamped rigid body poles ($g_2 < +\ 0.0113$), and

$$\frac{BM}{V_w}(s) = K\ \frac{s(s+c)(s+d)}{(s+\alpha)(s+\beta)(s+\gamma)} \tag{20}$$

for overdamped rigid body poles ($g_2 > +\ 0.0113$)

where:

$$K = \frac{1}{V}\cdot\frac{n_3}{d_3}$$

$$N_2 = \frac{n_2}{n_3}$$

$$N_1 = \frac{n_1}{n_3}$$

$$D_2 = \frac{d_2}{d_3}$$

$$D_1 = \frac{d_1}{d_3}$$

$$D_o = \frac{d_o}{d_3}$$

$$c^* = \frac{N_2}{2},\quad \omega_c^{\,2} = N_1 - \frac{N_2^2}{4}$$

$$c = \frac{N_2}{2} - \frac{1}{2}\sqrt{N_2^2 - 4N_1}$$

$$d = \frac{N_2}{2} + \frac{1}{2}\sqrt{N_2^2 - 4N_1}$$

$$\alpha = \frac{D_o}{D_1}$$

$$\beta^* = \frac{D_2}{2}, \quad \omega_\beta^2 = D_1 - \frac{D_2^2}{4}$$

$$\beta = \frac{D_2}{2} - \frac{1}{2}\sqrt{D_2^2 - 4D_1}$$

$$\gamma = \frac{D_2}{2} + \frac{1}{2}\sqrt{D_2^2 - 4D_1}$$

It should be recalled that: (1) The pole-zero pair of $\frac{BM}{V_w}(j\omega)$ in the high frequency region, i.e. the d-γ zero-pole pair, dominates the bending moment response of the rigid booster model, and (2) the bending moment magnitude in the low frequency range in response to lateral wind disturbances are increasingly attenuated as positive lateral acceleration feedback is increased. Thus, the approximate $\frac{BM}{V_w}(s)$ transfer function of equation (20) is simplified to

$$\frac{BM}{V_w}(j\omega) \doteq K \frac{(s+d)}{(s+\gamma)} \tag{21}$$

where K, d, and γ are given in equation (20). Bode plot of the simplified $\frac{BM}{V_w}(j\omega)$ transfer function is shown in Figure 6.

Statistical Analysis of the Rigid Booster

The adoption of statistical techniques to compute the vehicle responses to lateral wind disturbances was a convenient method for correlating and evaluating the exact and simplified transfer functions. For this purpose, two simplifying assumptions were made: (1) The vehicle system equations are linear time-invariant for time equal eighty seconds after launch, and (2) the lateral wind input is a stationary random process that can be roughly approximated by the well known Press atmospheric turbulence spectra.

For a linear time-invariant system, Laning and Battin have shown that the mean-square system output, σ^2, is simply

$$\sigma^2 = \int_0^\infty G_{YY}(\omega)d\omega$$

$$= \int_0^\infty \left| Y(j\omega) \right|^2 G_{V_w V_w}(\omega)d\omega \qquad (22)$$

where: $G_{YY}(\omega)$ = system output spectra

$G_{V_w V_w}(\omega)$ = wind input spectra

$Y(j\omega)$ = system frequency response function.

The mean-square lateral drift velocity response is then

$$\sigma^2_{\dot{Y}} = \int_0^\infty \left| \frac{\dot{Y}}{V_w}(j\omega) \right|^2 G_{V_w V_w}(\omega)d\omega, \qquad (23)$$

and the mean-square bending moment response

$$\sigma^2_{BM} = \int_0^\infty \left| \frac{BM}{V_w}(j\omega) \right|^2 G_{V_w V_w}(\omega)\, d\omega. \qquad (24)$$

Application of equation (22) to determine the variance (mean-square response) demands stationarity of both the system responses and system inputs. Derivation of the system transfer functions for a fixed time of flight configuration assures stationarity of system characteristics. An approximation to the lateral wind characteristics is assumed to be of the form suggested by Press and Meadows and is represented by the one-dimensional stationary spectra following:

$$G_{V_w V_w}(\omega) = \frac{\sigma_w^2 L}{\pi V} \frac{1 + 3L^2 \left|\frac{\omega}{V}\right|^2}{\left[1 + L^2 \left|\frac{\omega}{V}\right|^2\right]^2} \tag{25}$$

where: σ_w = variance of the wind turbulence velocities

L = integral scale of the turbulence

This spectra is plotted in Figure 7 for $\sigma_w = 2.5$, $L = 1000$

Computation of the exact and simplified mean-square lateral drift velocities, $\sigma^2_{\dot{Y}}$, was accomplished using equation (23), by the following procedure:

(1) $40 \log \left|\frac{\dot{Y}}{V_w}(j\omega)\right|$ (Figures 3, 5) was summed with $20 \log \left|G_{V_w V_w}(j\omega)\right|$ (Figure 7) and plotted on a linear frequency scale in Figure 8 to obtain the lateral drift output power spectra, $G_{\dot{Y}\dot{Y}}(\omega)$, for various values of accelerometer gain, g_2.

(2) The area underlying $G_{\dot{Y}\dot{Y}}(\omega)$ was integrated with a planimeter to obtain the mean-square lateral drift velocity. The same procedure, using equation (24) and Figures 4, 6, and 7, was used to compute the mean-square bending moment, σ^2_{BM}, from the output power spectra, $G_{BM\text{-}BM}(\omega)$, shown in Figures 9-10.

EVALUATION OF SIMPLIFIED TRANSFER FUNCTIONS

Evaluation of the simplified lateral drift and bending moment transfer functions developed in this study utilizes the mean-square $\dot{Y}$ and BM outputs as a performance index. The root-mean-squared values of $\dot{Y}$ and BM may be interpreted as values of these quantities which occur approximately 67 percent of the time.

Comparison of $\sigma_{\dot{Y}}$ and σ_{BM} values obtained from their exact and simplified transfer functions, for the nominal configuration ($a_o = .48$, $a_1 = 1.1$) and varying lateral acceleration feedback, is shown in Figure 11. Negligible error is perceptible in $\sigma_{\dot{Y}}$ as determined from the exact and simplified expressions for $\frac{\dot{Y}}{V_w}(j\omega)$. σ_{BM} obtained from $\frac{BM}{V_w}(j\omega)$ simplified exceeds σ_{BM} of the exact $\frac{BM}{V_w}(j\omega)$ transfer function by approximately 5 percent. It is felt that the maximum error exhibited by the simplified bending moment transfer function is not of sufficient magnitude as to offset the insight it lends to the complicated minimum load control problem. Thus, the simplified lateral drift and bending moment transfer functions possess the advantage of approximating their exact expressions within acceptable error, with an attendant clarity which aids in determination of the basic criteria for minimum drift and minimum load control.

CRITERIA FOR MINIMUM DRIFT AND MINIMUM LOAD CONTROL

Minimum drift and minimum load control criteria, for the mathematical booster model considered in this study, are stated below.

Minimum Drift

(1) Vehicles lateral drift response to lateral wind disturbance is dominated by the lateral drift pole (i.e., the negative, real pole close to the origin) of the closed-loop $\frac{\dot{Y}}{V_w}(s)$ transfer function.

(2) The lateral drift pole is approximately

$$s = -\alpha \doteq -\frac{d_o}{d_1} \tag{24}$$

where: $d_1 = m(X_E F_s a_o + Q F_1) + (X_E F_s Q F_o - F_s Q F_1)(\frac{a_1}{V} + g_2)$

$$d_o = \frac{1}{V}\left[(X_E F_s Q F_o - F_s Q F_1)(a_o - g_2 g) - mgQF_1\right]$$

(3) Minimum lateral drift is accomplished by driving the lateral drift pole, α, close to the origin, i.e., when $d_o \to 0$. The lateral acceleration feedback satisfying this condition for minimum drift, in the limit, tends to

$$g_2 = \frac{a_o}{g} - \frac{mF_1}{F_s(X_E F_o - F_1)} \approx .038 \tag{25}$$

(4) Increases in pitch heading gain, a_o, and pitch damping gain, a_1, affect the lateral drift pole as shown in Figure 12.

Minimum Load

(1) Bending moment response to lateral wind disturbance exhibits a

trade-off about the control frequency, i.e., positive lateral acceleration feedback attenuates the bending moment for frequencies less than $\omega \doteq 1$ rad/sec while it amplifies the bending moment for frequencies greater than $\omega \doteq 1$ rad/sec; negative acceleration feedback reverses the effect.

(2) The simplified rigid body transfer function is

$$\frac{BM}{V_w}(s) \doteq K \frac{s+b}{s+\gamma} ; \tag{26}$$

this rigid body zero-pole pair, b-γ, is located in the frequency region above $\omega \doteq 1$ rad/sec, and dominates the bending moment response. Increases in lateral acceleration feedback cause b and γ to separate, resulting in a favorable effect on structural load reduction below $\omega \doteq 1$ rad/sec, and a detrimental effect above $\omega \doteq 1$ rad/sec.

(3) Bending moment trade-off-wind input intereffects, particularly if higher order dynamics are considered, cloud the determination of specific criteria for minimizing structural loading, i.e., specific criteria for minimum load control depend primarily on the lateral wind spectra.

CONCLUSIONS

The major conclusions which may be drawn from this re-evaluation of criteria for minimum drift and minimum load control are:

(1) Simplified lateral drift and bending moment closed-loop transfer functions developed in this study approximate their exact transfer functions with negligible error.

(2) These simplified transfer functions clarify the dominant effects which system parameter changes have on minimizing lateral drift and structural loading.

(3) Minimum drift control is easily specified by positioning a single root of the vehicle characteristic equation.

(4) Minimum load control criteria are obscurely defined in terms of the interrelation which exists between the rigid body control frequency trade-off and the lateral wind disturbance spectra.

While studies to date suggest the trade-off effect on structural loading is small, this indication is obtained using wind spectra of, as yet, undetermined quality to represent actual wind spectra. In addition, insertion of initial conditions and including parameter changes with time neglected in this study, could conceivably alter the current emphasis on the trade-off effect. A better resolution of minimum load control criteria as influenced by minimum drift control, based on procedures developed herein, is dependent upon a better definition of actual wind spectra characteristics at various flight times.

REFERENCES

1. Townsend, Don, Saturn V Wind Response Studies, MTP-AERO-63-63, George C. Marshall Space Flight Center, September 10, 1963.

2. Bailey, J. E., Launch Vehicle Wind Response by Statistical Methods. Hayes International Corporation, Engineering Report No. 1193, November 29, 1965.

3. Press, Harry, Atmospheric Turbulence Environment with Special Reference to Continuous Turbulence. Report No. 115, Advisory Group for Aeronautical Research and Development, April-May 1957.

4. Press, H., M. T. Meadows and I. Hadlock. A Re-evaluation of Data on Atmospheric Turbulence and Airplane Gust Loads for Application in Spectral Applications. NACA Report 1272, 1956.

5. Clingan, Bruce E., Dynamic Loads Due to Wind Shear. AIAA Journal, Volume 2, Number 1, January 1964. pp. 76-84.

6. Townsend, Don, A Method for the Determination of Control Law Effect on Vehicle Bending Moment. NASA TM X-53077.

7. Bieber, R. E., Missile Structural Loads by Nonstationary Statistical Methods. Journal of the Aerospace Sciences, Volume 28, Number 4, April 1961, pp. 284-294.

8. Lukens, David R., Alfred F. Schmitt and George T. Broucek. Approximate Transfer Functions for Flexible Booster and Autopilot Analysis. WADD TR-61-93, April 1961.

9. Lester, Harold C., and Homer G. Morgan. Determination of Launch Vehicle Response to Detailed Wind Profiles. Journal of Spacecraft and Rockets, Volume 2, Number 1, January-February 1965.

10. Mazzola, Luciano L. Design Criteria for Wind-Induced Flight Loads on Large Boosted Vehicles. AIAA Journal (Technical Notes and Comments), Volume 1, Number 4, April 1963, pp. 913-914.

11. Goldman, Robert. A Method for Predicting Dynamic Response of Missiles to Atmospheric Disturbances. IAS Paper No. 62-40.

12. Scoggins, James R., and William W. Vaughan. Problems of Atmospheric Wind Inputs for Missile and Space Vehicle Design. Journal of Spacecraft and Rockets, Volume 1, Number 2, March-April 1964, pp. 181-184.

REFERENCES

Continued

13. Scoggins, James R., and William W. Vaughan. Some Properties of Atmospheric Turbulence for Space Vehicles. Aerospace Environment Office, Aero-Astrodynamics Laboratory, NASA-George C. Marshall Space Flight Center, June 1965.

14. Lester, Harold C., and Dennis F. Collins, Determination of Loads on a Flexible Launch Vehicle During Ascent Through Winds. NASA TN-D-2590. February 1965.

15. McWaters, S. R., and J. E. Bailey. Stability Investigation of Multi-Accelerometer Control of Large Flexible Booster Vehicles. Hayes International Corporation, Engineering Report No. 1054, August 20, 1964.

16. Laning, J. Halcombe, and Richard H. Battin. Random Processes in Automatic Control. New York: McGraw-Hill Book Company, Inc., 1956.

17. Truxal, John G. Automatic Feedback Control System Synthesis. New York: McGraw-Hill Book Company, Inc., 1955.

18. D'Azzo, J. J., and C. H. Houpis. Feedback Control System Analysis and Synthesis. New York: McGraw-Hill Book Company, Inc., 1960.

19. Crandall, Stephen H. Random Vibration, Volume 2, Cambridge, Mass.: M.I.T. Press, 1963.

20. Etkin, Bernard. Dynamics of Flight. New York: John Wiley and Sons, Inc. 1959.

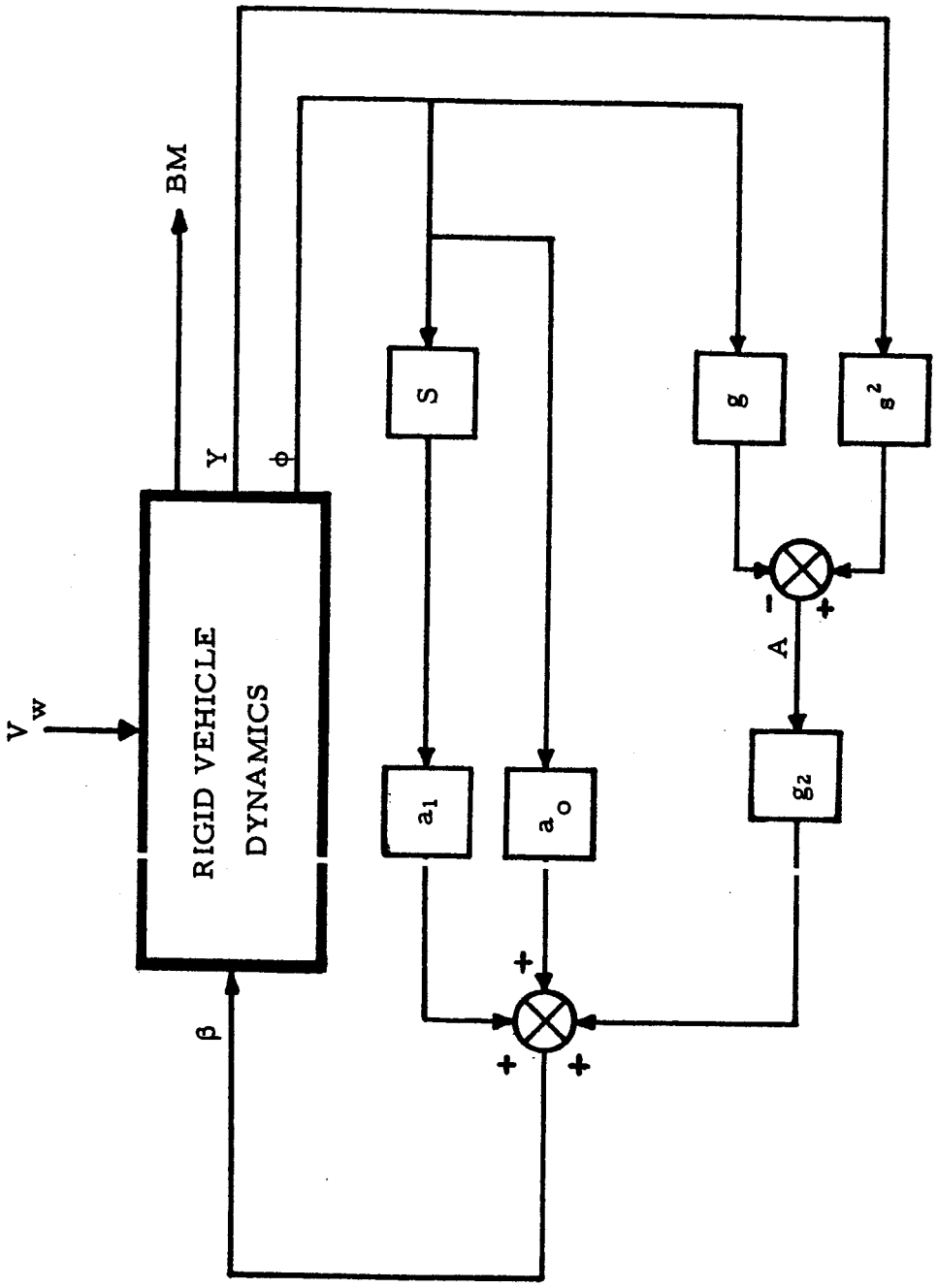

FIGURE 1 CONTROL SYSTEM BLOCK DIAGRAM

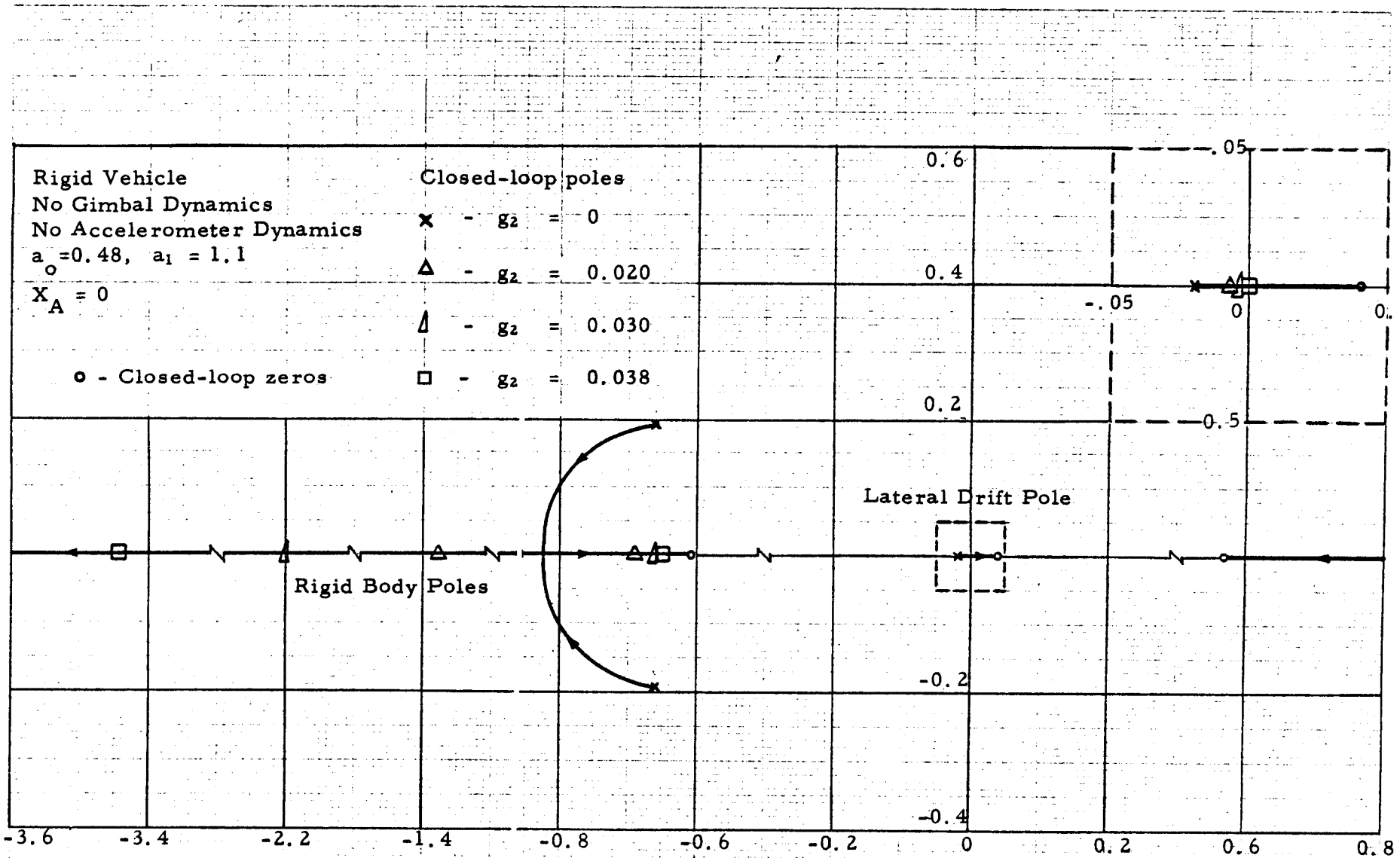

FIGURE 2 EFFECT OF POSITIVE LATERAL ACCELERATION FEEDBACK ON CLOSED-LOOP POLES OF Δ

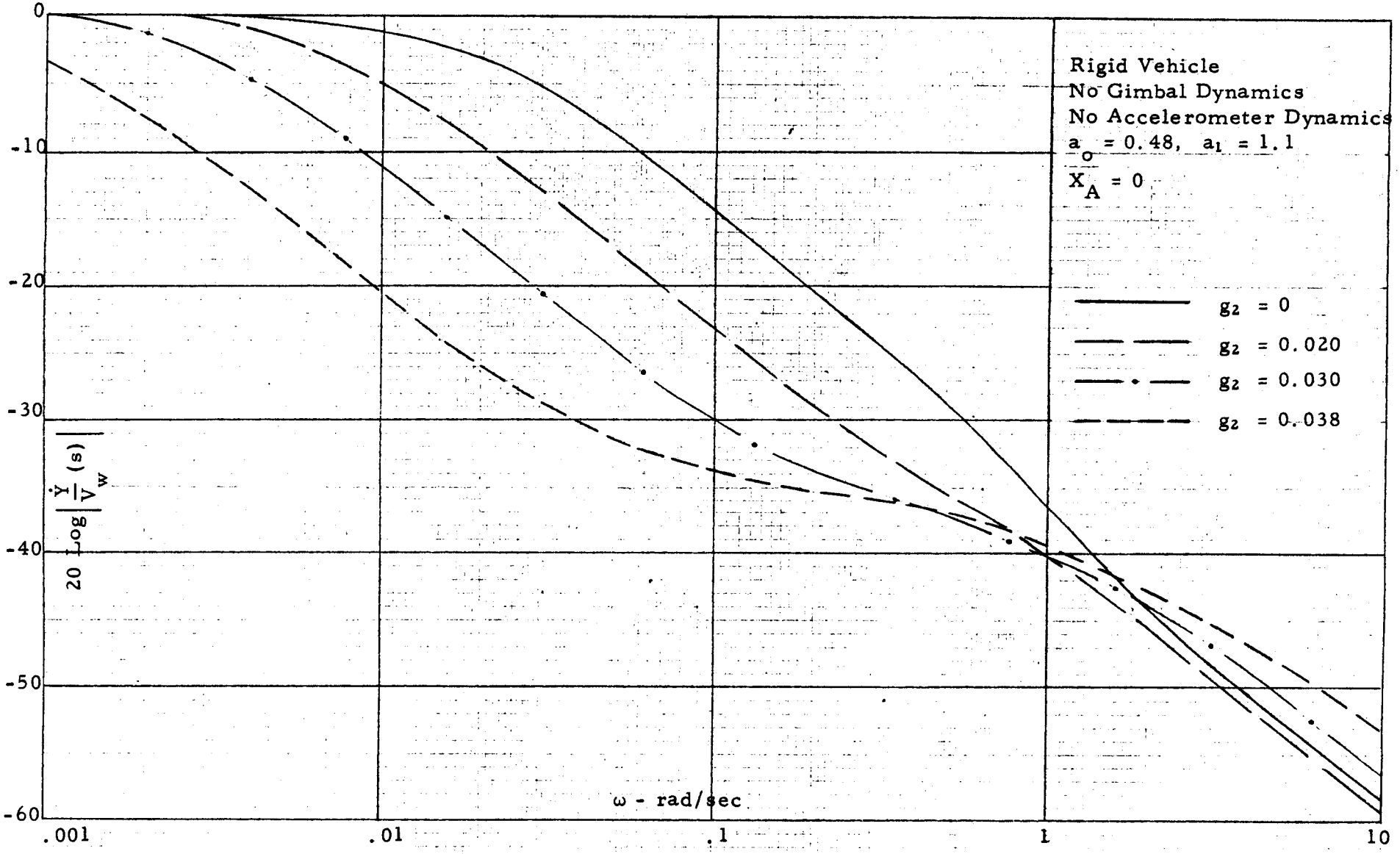

FIGURE 3 BODE PLOT OF EXACT $\frac{\dot{Y}}{V_w}(s)$ TRANSFER FUNCTION SHOWING EFFECT OF ACCELERATION FEEDBACK

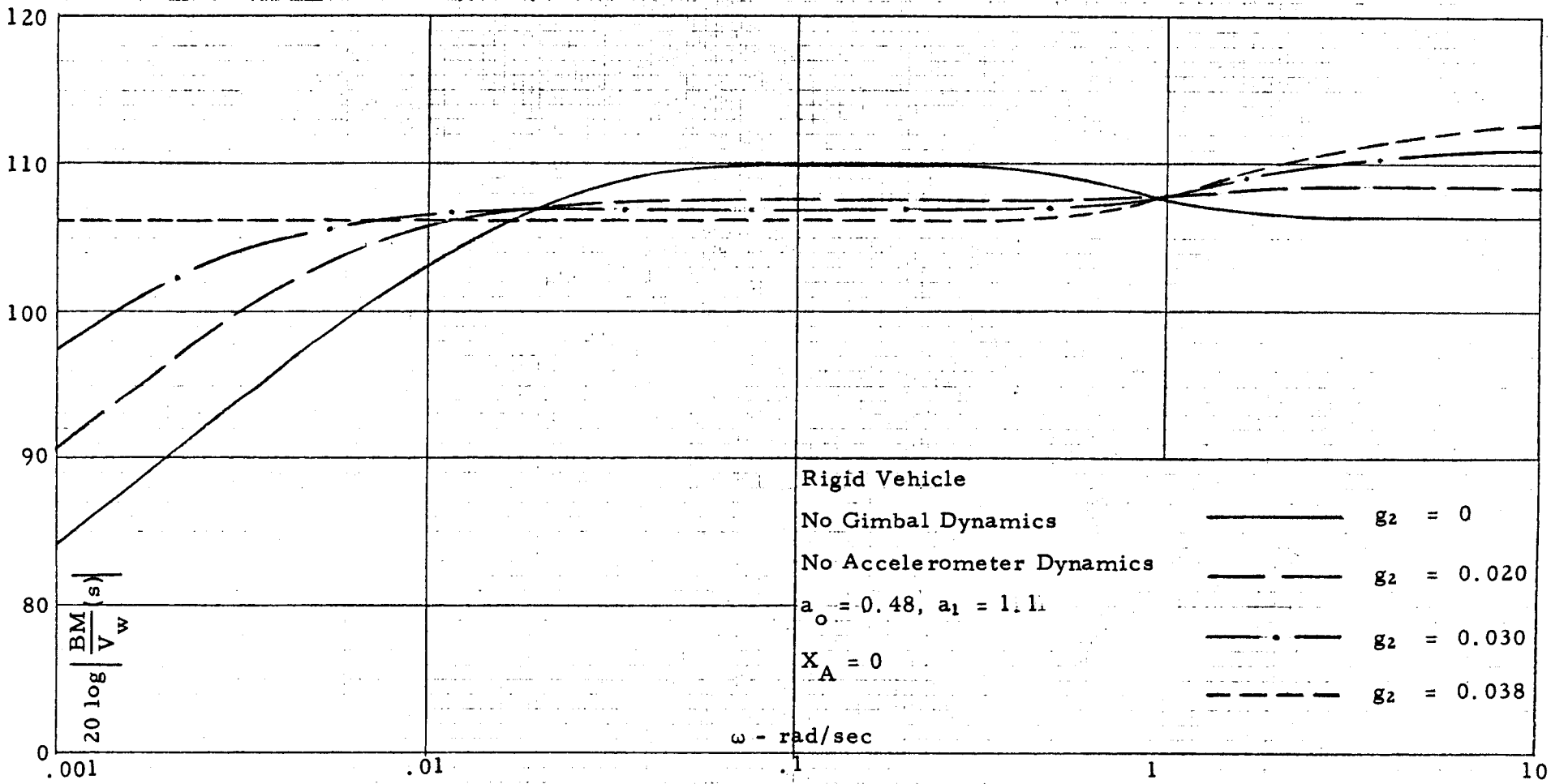

FIGURE 4 BODE PLOT OF EXACT $\frac{BM}{V_w}(s)$ TRANSFER FUNCTION SHOWING EFFECT OF ACCELERATION FEEDBACK

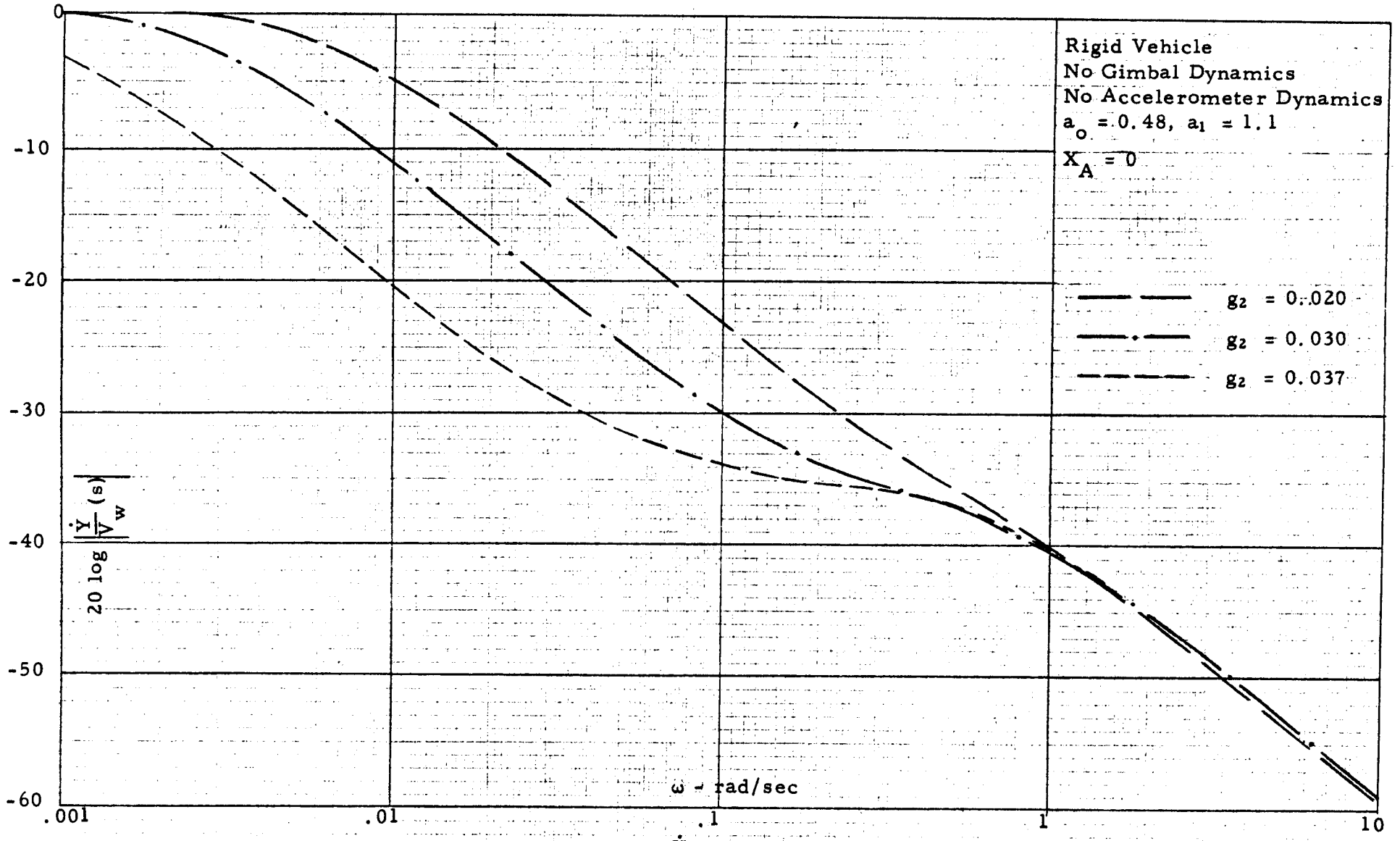

FIGURE 5 BODE PLOT OF SIMPLIFIED $\frac{\dot{Y}}{V_w}(s)$ TRANSFER FUNCTION SHOWING EFFECT OF ACCELERATION FEEDBACK

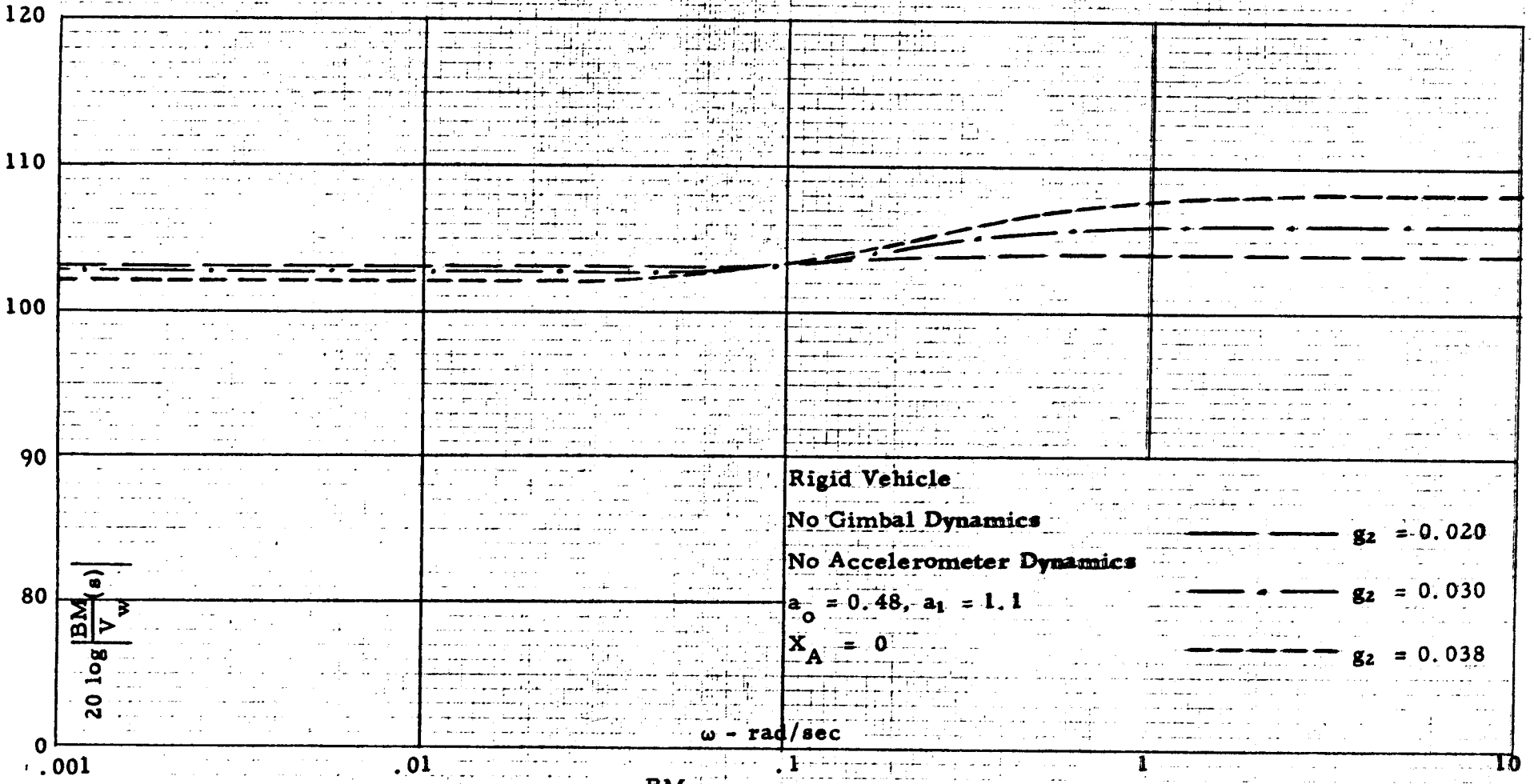

FIGURE 6 BODE PLOT OF SIMPLIFIED $\frac{BM}{V_w}(s)$ TRANSFER FUNCTION SHOWING EFFECT OF ACCELERATION FEEDBACK

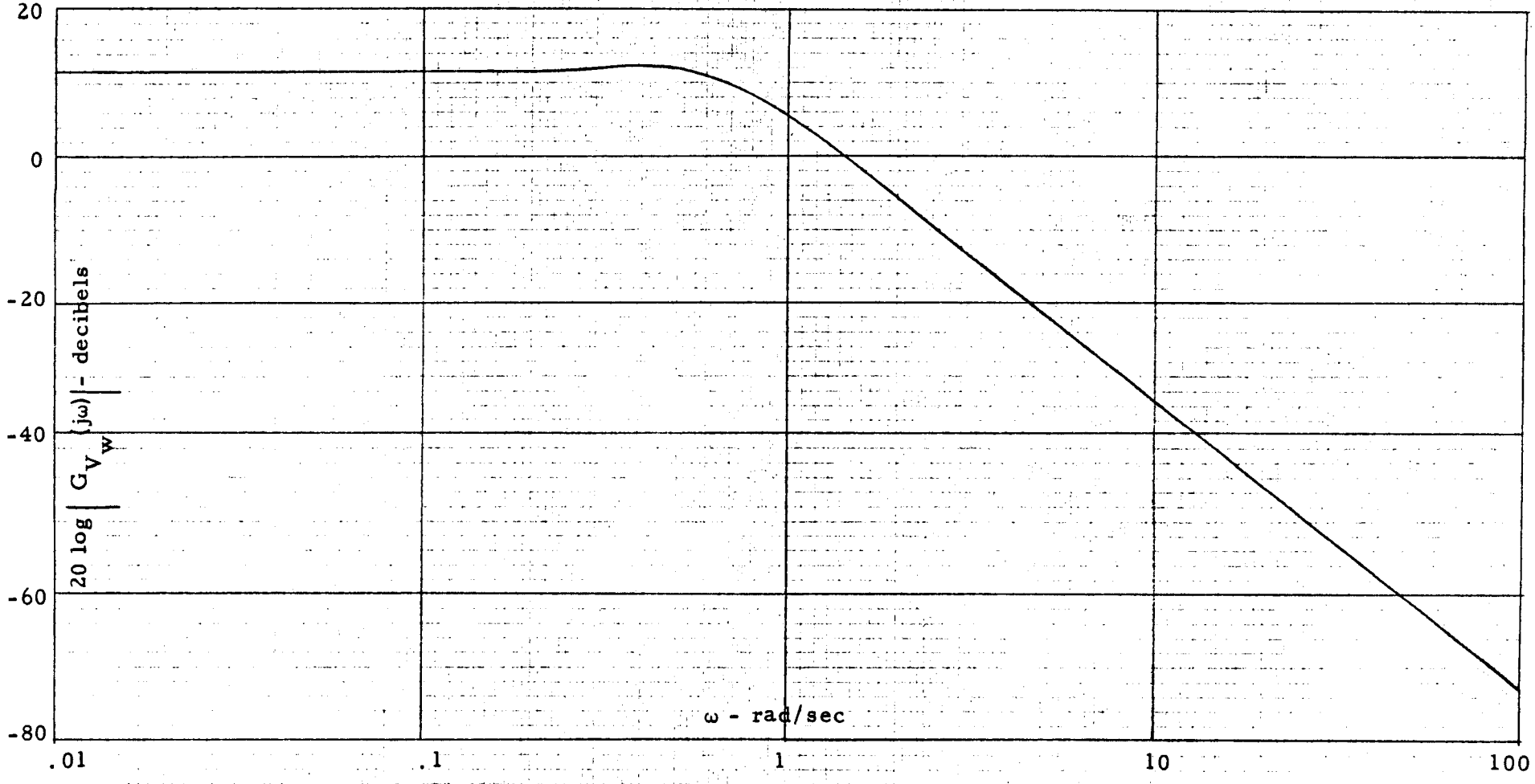

FIGURE 7 TYPICAL POWER SPECTRA OF ATMOSPHERIC TURBULENCE
(σ = 2.5, L = 1000)

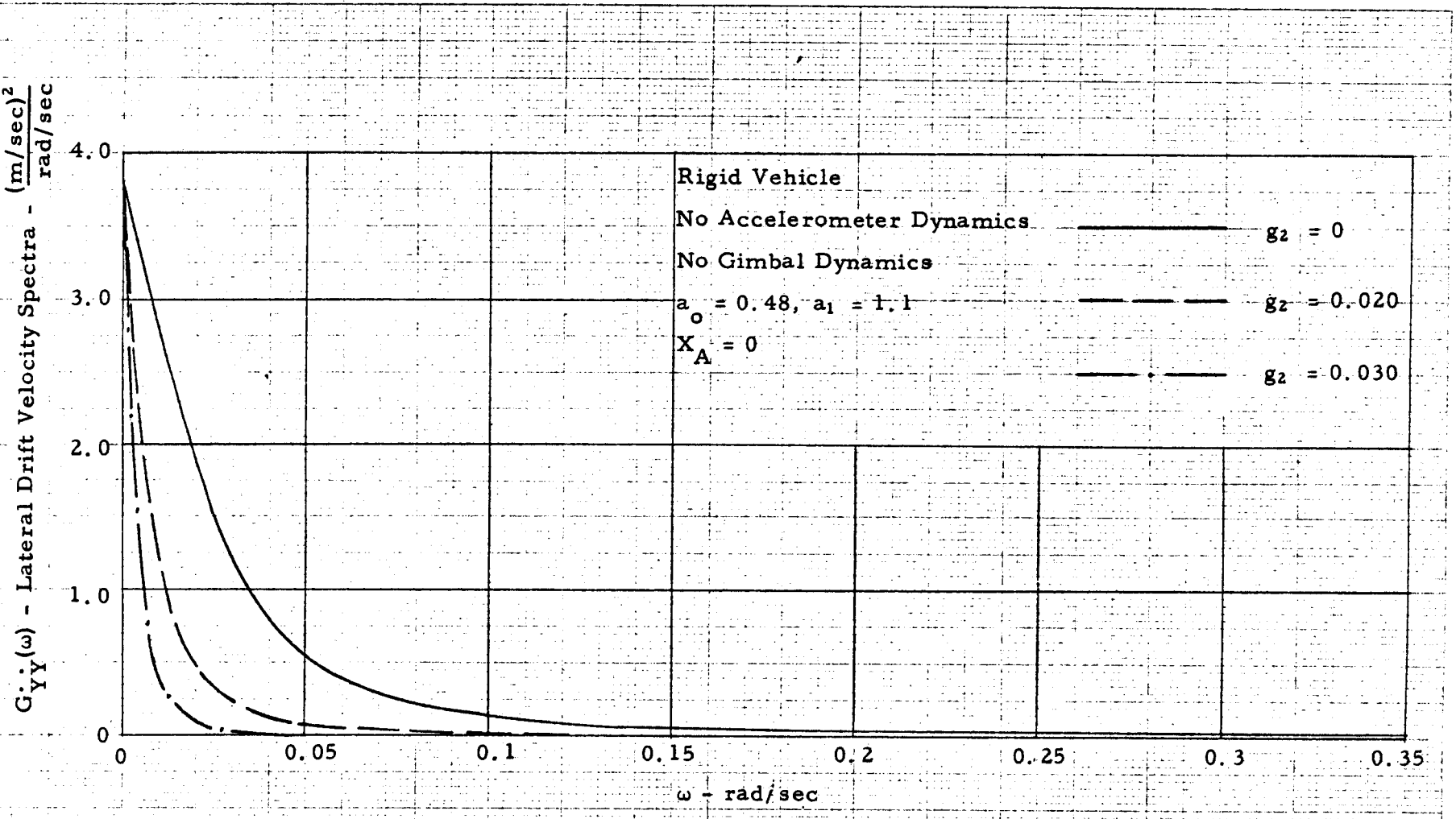

FIGURE 8 EXACT AND SIMPLIFIED LATERAL DRIFT VELOCITY OUTPUT POWER SPECTRA

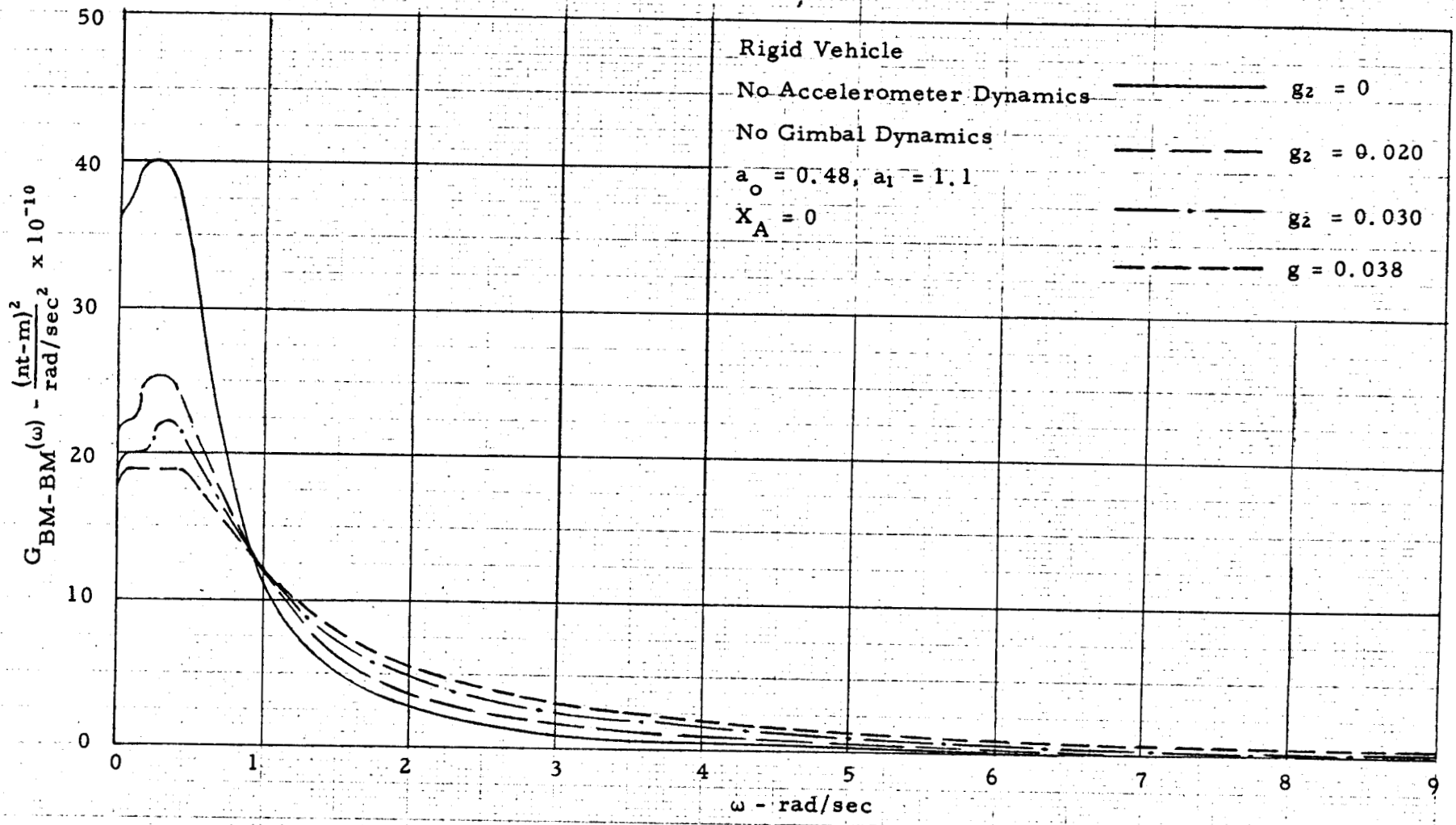

FIGURE 9 EXACT BENDING MOMENT OUTPUT POWER SPECTRA

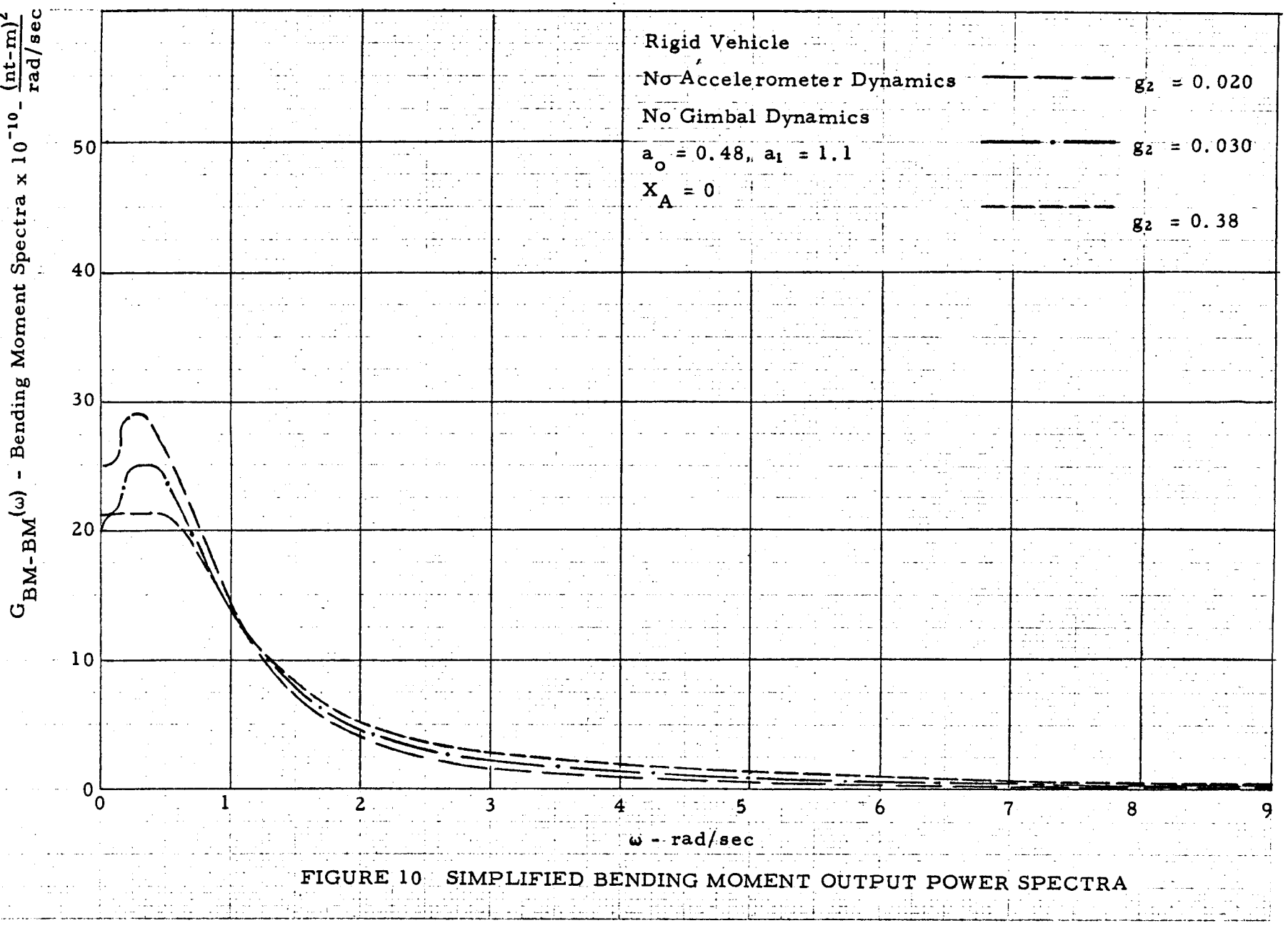

FIGURE 10 SIMPLIFIED BENDING MOMENT OUTPUT POWER SPECTRA

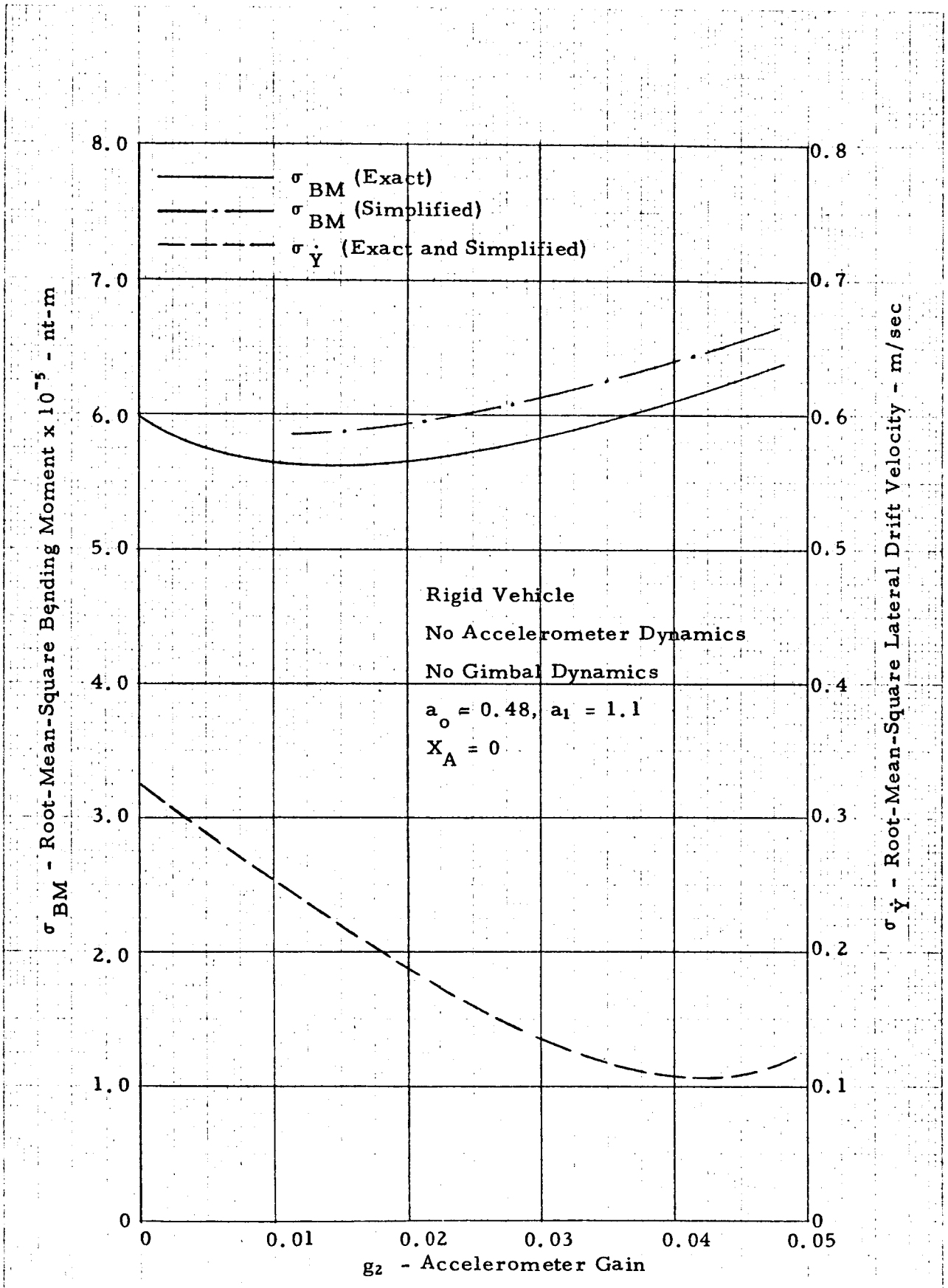

FIGURE 11 EFFECT OF LATERAL ACCELERATION FEEDBACK ON ROOT-MEAN-SQUARE LATERAL DRIFT VELOCITY AND RIGID BODY BENDING MOMENT (σ = 2.5, L = 1000)

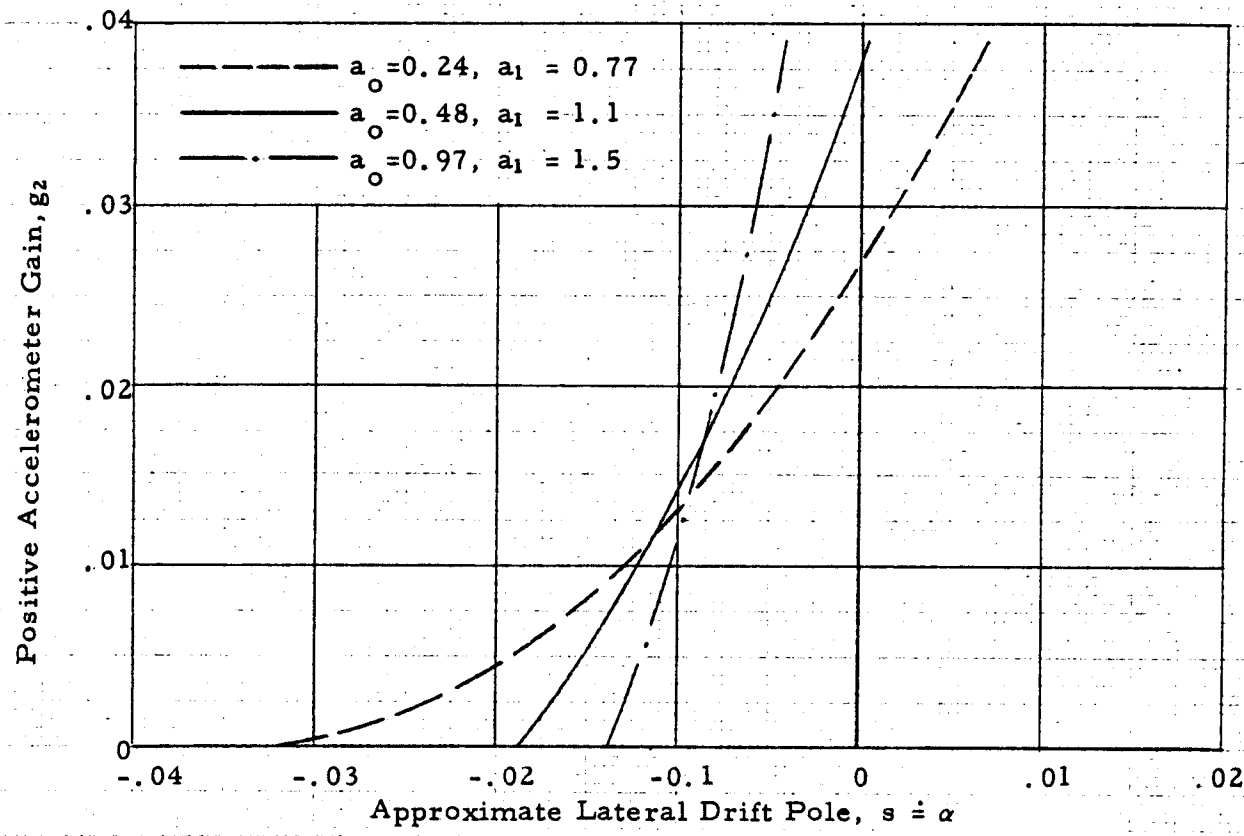

FIGURE 12 EFFECT OF PITCH HEADING AND PITCH DAMPING GAINS ON APPROXIMATE LATERAL DRIFT POLE